Journal of Chromatography A, 1218 (2011) 907–921

Contents lists available at ScienceDirect

Journal of Chromatography A

journal homepage: www.elsevier.com/locate/chroma

The mass transfer kinetics in columns packed with Halo-ES shell particles

Fabrice Gritti, Georges Guiochon*

Department of Chemistry, University of Tennessee, Knoxville, TN 37996-1600, USA

ARTICLE INFO

Article history:
Received 29 June 2010
Received in revised form
29 November 2010
Accepted 13 December 2010
Available online 24 December 2010

Keywords:
Column packing technology
Shell particles
Van Deemter curve
HETP
Halo-C_{18}
Insulin
Lysozyme
β-Lipotropin
Uracil
Acetophenone
Toluene
Naphthalene
Polystyrene standard

ABSTRACT

The average mesopore size of the new Halo-ES-Peptide shell particles is 160 Å, markedly larger than that of the classical Halo shell particles (90 Å). We found that this change causes a considerable decrease of the film mass transfer resistance measured for columns packed with these particles. We analyze data obtained by systematic measurements of the *C* term of the van Deemter equation for the peptide β-lipotropin (MW = 769 Da), the protein insulin (MW = 5800 Da), and a series of non-retained polystyrene standards (MW = 6400 and 13,200). The improvement in column performance is explained by an increase of the fraction of the external surface area of the shell that allows the entrance of the sample molecules inside the particle. The fraction of the shell surface accessible to a probe controls the rate of its external film mass transfer, i.e. its rate of transfer between the interstitial and the stagnant eluent. Although measurable, the increase in sample diffusivity through the porous shells does not account for the better performance of Halo-ES-peptide columns. Furthermore, the analysis of the HETPs data of small molecules (uracil, acetophenone, toluene, and naphthalene, *MW* < 150) reveals that the eddy diffusion (*A*) term of these new columns is 25% lower than that of the classical Halo columns. This result is consistent with the impact of intra-particle diffusivity on the eddy diffusion mechanism in packed columns. As shell diffusivity increases, so does the rate of transfer of sample molecules between the eluent stream-paths flowing through the packed particles and across the column diameter. Dispersion through short-range inter-channel and trans-column eddies is reduced.

1. Introduction

Superficially porous particles were first introduced in liquid chromatography in 1967 when Horvath and Lipsky prepared large silica bead (50–100 μm) coated with a thin layer of ion-exchange resin to separate nucleotides [1,2]. Only few similar packing materials were prepared and commercialized during the next 40 years [3,4]. They were supposed to be coated with a liquid or a polymer, which were insoluble in the mobile phase and to be used in liquid–liquid chromatography. This approach eventually failed and HPLC was implemented as liquid-solid chromatography, using smaller and smaller fully porous particles. Superficially porous particles were forgotten until 4 years ago, when Kirkland et al. introduced the 2.7 μm Halo particles [5,6]. Columns packed with these particles exhibited minimum reduced plate heights of 1.4 and HETP's of 2.7 × 1.4 = 3.8 μm, nearly equivalent to those generated by columns packed with 1.7 μm fully porous particles, e.g. 2.0 × 1.7 = 3.4 μm [7,8]. Last year, Phenomenex introduced columns packed with 2.6 μm Kinetex shell particles, which achieved minimum plate heights of 1.2 × 2.6 = 3.2 μm, an unprecedented achievement for 4.6 mm I.D. commercial columns [9–11]. While lower plate heights could be generated with capillary columns packed with sub-1 μm particles [12], commercial columns packed with sub-3 μm shell particles have the great advantage of working with conventional LC systems, provided that some minor modifications of the extra-column parts of current commercial instruments (needle seat capillary, connecting tubes, detector cell) [13,14].

Interestingly, it was recently shown that the enhanced performance of columns packed with shell particles in the separation of small molecules was due to the combination of lower longitudinal diffusion (*B* coefficient) and eddy diffusion (*A* coefficient) terms of the general van Deemter equation [15]. Most noteworthy, the shell structure of these particles has no effect on the resolution of small molecular weight compounds because these compounds diffuse most rapidly, so trans-particle mass transfer resistance in fully porous particles is nearly negligible and does not contribute significantly to the overall plate height around the minimum of the HETP curve [16]. The mass transfer resistance at the solid–liquid interface is mostly accounted for by the external film mass transfer resistance [17,18] and, possibly, by the heat friction under very high pressures [19,20].

* Corresponding author. Tel.: +1 865 974 0733; fax: +1 865 974 2667.
E-mail address: guiochon@utk.edu (G. Guiochon).

0021-9673/$ – see front matter © 2010 Elsevier B.V. All rights reserved.
doi:10.1016/j.chroma.2010.12.046

The B coefficient of columns packed with shell particles is usually ca. 25% lower than that of columns packed with fully porous particles because diffusion is strictly zero in the non-porous silica cores. The diameters of the cores of Halo, Kinetex and Poroshell 120 are about 70% that of the particles [15]. Therefore, the core volumes represent 35% of the particle volume and about 20% of the column tube volume, hence the lower B term. The A term of columns packed with shell particles is usually 40% smaller than that of those packed with fully porous particles [15,16], due to a decrease of the short-range inter-channel and trans-column velocity biases. Short-range eddies are reduced, either due to the tight size distribution of the shell particles, which typically have a relative standard deviation (RSD) of about 5%, or due to the slightly rougher external surface area of the shell particles, which reduces the amplitude of the strain distribution taking place during bed consolidation [21]. They pack into beds that are highly homogeneous at a length scale of a few particle diameters.

When it comes to separate high molecular weight compounds such as proteins or polymers, which have low diffusivities, column performance is determined by the value of the C coefficient. We recently reported that the efficiency for insulin of Halo-C_{18} columns was significantly smaller than that of Kinetex-C_{18} columns [9]. Yet, these columns provide a similar resolution for low molecular weight compounds and have the same mesopore size ($\simeq$ 90–100 Å). Insulin is a 5.8 kDa molecular weight protein with a diffusion coefficient of 1.6×10^{-6} cm^2/s in the eluent used and a hydrodynamic radius of 32 Å [22,23]. Inverse size exclusion chromatography (ISEC) made clear that the porosities of the shells of the two particles are different (0.51 and 0.20 for Kinetex-C_{18} and Halo-C_{18}, respectively [15]). This suggested that the silica walls and/or the hydrophobic C_{18}-bonded layer in the shells are thicker for the Halo than for the Kinetex particles. Although both porous shells have the same average pore size, the C coefficient of the Halo column is nearly five times larger than that of the Kinetex column, consistent with the statement that the Halo 90 Å column was not designed to separate large molecular weight compounds [5] and with its success in separating small molecular weight ones.

In early 2010, Kirkland et al. [24] described the properties of columns packed with new Halo particles having a larger average mesopore size of 160 Å and Advanced Materials Technology released these columns as Halo-ES peptide. In this work, we compare the mass transfer kinetics in Halo 90 Å and 160 Å for four small molecules (uracil MW = 112, acetophenone MW = 120, toluene MW = 92, and naphthalene MW = 128), one peptide (β-lipotropin MW = 769, Ala-Ala-Ala-Tyr-Gly-Gly-Phe-Leu, MW = 769), two proteins (insulin MW = 5808 and lysozyme MW = 14,700), and six unretained polystyrene standards (MW = 1100, 6400, 13,200, 31,600, 90,000, and 171,000). The causes of the improvement in the mass transfer kinetics observed for the larger molecules are discussed and a physical explanation proposed.

2. Theory

2.1. Reduced linear velocity

In all this work, we report the reduced plate height h of the columns as a function of the reduced interstitial velocity ν. By definition,

$$\nu = \frac{u d_p}{D_m}, \qquad h = \frac{H}{d_p} \tag{1}$$

where H is the column HETP, d_p the average particle size of the packing material, D_m is the bulk molecular diffusivity, and u the interstitial linear velocity given by:

$$u = \frac{F_v}{\epsilon_e \pi R_c^2} \tag{2}$$

where F_v is the volume flow rate of the mobile phase, ϵ_e the interstitial porosity, and R_c the inner radius of the column tube.

The molecular diffusivities in the eluent of the low-molecular-weight compounds used here (uracil, acetophenone, toluene, naphthalene) were estimated with the classical Wilke and Chang equation [25] extended to mixture of eluents [26] (see Eqs. (11)–(12.3)):

$$D_m = 7.4 \times 10^{-8} \frac{(x_{ACN}\Psi_{ACN}M_{ACN} + x_{H_2O}\Psi_{H_2O}M_{H_2O})^{0.5} T}{\eta V_A^{0.6}} \tag{3}$$

where Ψ is the solvent association factor (Ψ_{ACN} = 1 and Ψ_{H_2O} = 2.6 [26]), M_{ACN} =41 g/mol and M_{H_2O} =18 g/mol are the molecular weight of acetonitrile and water, x_{ACN} and x_{H_2O} are the molar fractions of acetonitrile and water in the eluent used, η the viscosity of the mobile phase (η = 0.54 and 1.04 cP for two mixtures of acetonitrile and water (80/20 and 31/69, respectively, v/v) at 295 K, respectively), T is the temperature, and V_A the molar volume of the solute at its boiling point (V_A = 97.9, 140.2, 118.6, and 150.8 cm^3/mol for uracil, acetophenone, toluene, and naphthalene,, respectively). V_A was estimated according to the group method of Schroder and Lebas [26]. The correlation in Eq. 3 gives reasonable values of D_m, within a ± 10% estimated error. T is in Kelvin, η in centipoise, and MW in g/mol.

The diffusion coefficient of insulin was obtained from reference [23] (1.6×10^{-6} cm^2/s). The bulk molecular diffusion coefficients of the peptide β-lipotropin and of the protein lysozyme were estimated using the Young correlation [27]:

$$D_m = 8.34 \times 10^{-8} \frac{T}{\eta MW^{\frac{1}{3}}} \tag{4}$$

In Eq. 4, T, η, and MW are expressed in Kelvin, centipoise, and Dalton, respectively.

The bulk molecular diffusivities of the polystyrene standards in pure THF, at 295 K were obtained from [22] using the following correlation:

$$D_m = 3.45 \times 10^{-4} \times MW^{-0.564} \tag{5}$$

2.2. Reduced HETP terms

In a general sense, the overall reduced HETP of a chromatographic column is the sum of five main contributions due to (1) longitudinal diffusion (the B term); (2) eddy diffusion (the A term); (3) the external film mass transfer resistance (the C_f term); (4) the trans-particle mass transfer resistance (the C_p term); and (5) an additional contribution due to the heat friction of the eluent percolating across the bed, the h_{Heat} term [28–30].

$$h = \frac{B}{\nu} + A(\nu) + C_f\nu + C_p\nu + h_{Heat} \tag{6}$$

The term h_{Heat} is negligible at small flow rates, for weakly adsorbed compounds, eluents with high thermal conductivities, and under adiabatic conditions [8]. In this work, we operated with rather low retention factors (<2) and under nearly adiabatic conditions by keeping the column in the oven compartment of the instrument. Next, we explain how the terms B/ν, $C_p\nu$, and $C_f\nu$ were obtained for small molecules.

2.2.1. The longitudinal diffusion term

The B coefficient is directly derived from the results of peak parking experiments, e.g. from the slope, ($\Delta\sigma_{pp}^2/\Delta t_p$) of the peak

variance σ^2_{PP} (in s^2) *versus* the peak parking time t_p (see experimental section for details on the peak parking method). Accordingly, the B term is written as [16]:

$$B = \frac{\Delta\sigma^2_{PP}}{\Delta t_p}\frac{1}{D_m}\frac{u^2_{PP}}{1+k_1} \quad (7)$$

where k_1 is the zone retention factor defined by [31]:

$$k_1 = \frac{1-\epsilon_e}{\epsilon_e}[\epsilon_p + (1-\epsilon_p)K](1-\rho^3) \quad (8)$$

where ϵ_e is the external porosity of the packed bed, ϵ_p the internal porosity of the shell, K the distribution constant (Henry's constant) of the porous shell, ρ the ratio of the diameter of the solid silica core to that of the particle, and u_{PP} the constant interstitial linear velocity at which the peak parking measurements were performed.

2.2.2. The solid–liquid trans-particle mass transfer resistance term

The determination of the coefficient C_p in the general mass transfer equation is semi-empirical. In a first step, the effective sample diffusivity, D_{eff}, in the porous shell of the particle is estimated from the results of experiments made under static conditions (no flow). Accordingly, a model of diffusion should be assumed to relate D_{eff} and the apparent axial diffusion coefficient, D_{axial}, along a column packed with a heterogeneous medium. As a first approximation, we assimilate packed beds and the parallel distribution of two homogeneous phases. The first phase in the column is the bulk eluent, in which the solute diffusion coefficient is $\gamma_e D_m$ (γ_e is the external obstruction factor). The second phase is the volume occupied by the porous shell filled with the eluent in which the solute diffusivity is D_p. According to a parallel diffusion model, D_{axial} is written [15]:

$$D_{axial} = \frac{\epsilon_e\gamma_e D_m + (1-\epsilon_e)D_p}{\epsilon_t(1+k')} \quad (9)$$

where k' is the conventional retention factor.

A second model of longitudinal diffusion in packed beds, based on the effective medium theory (EMT) of Laudauer [32] and extended to molecular diffusion [33], was recently derived in [34]:

$$D_{axial} = \frac{a + \sqrt{a^2 + (1/2)(D_p/D_m)}}{\epsilon_t(1+k')}D_m \quad (10)$$

with

$$a = \frac{1}{4}\left[3\epsilon_e - 1 + \frac{D_p}{D_m}(2-3\epsilon_e)\right] \quad (11)$$

The coefficient D_{axial} is directly derived from the peak parking data (with $2D_{axial} = BD_m$) [16]:

$$D_{axial} = \frac{\Delta\sigma^2_{PP}}{\Delta t_p}\frac{F_v^2}{2\epsilon_e^2\pi^2 R_c^4[1+k_1]^2} \quad (12)$$

where F_v is the flow rate set in the parking experiments to carry over the sample zone in and out of the column and, under static conditions, D_p is written as follows [15]:

$$D_p = (1-\rho^3)D_{eff} \quad (13)$$

The second step consists in deriving the coefficient C_p for superficially porous particles. This calculation was done long ago by Horvath et al. [2], based on the non-equilibrium theory of Giddings, which permits the derivation of the configuration factor of given distributions of the stationary phase to the mass transfer resistance [35]. Recently Kaczmarski et al. used the Laplace transform of the general rate model of chromatography [31] to perform this derivation and obtained the same result. Eventually, C_p is written:

$$C_p = \frac{1}{30}\frac{\epsilon_e}{1-\epsilon_e}\frac{k_1^2}{(1+k_1)^2}\frac{1+2\rho+3\rho^2-\rho^3-5\rho^4}{(1+\rho+\rho^2)^2}\frac{1}{\Omega} \quad (14)$$

In this equation, Ω is the ratio of the solute diffusivity in the shell, D_{eff}, to the bulk diffusion coefficient, D_m [36].

2.2.3. The solid–liquid external film mass transfer resistance term

Miyabe et al. [17] measured recently the external film mass transfer coefficient, k_f, for large porous silica-C_{18} particles and for small molecules. They could not measure k_f for sub-3 μm porous particles with a sufficient accuracy, due to the significant scatter of the HETP data (5% for retained analytes) and because the C terms of columns packed with these particles are extremely small. This study demonstrated that the Wilson and Geankoplis correlation for k_f [18] accounts satisfactorily for the exchange rate of solute molecules between the moving eluent in the inter-particle space and the stagnant eluent inside the porous particles. In this work, we assume that this correlation extend to sub-3 μm superficially porous particles. Accordingly, the coefficient C_f in the general equation 6 is given by the Laplace transform of the general rate model solution [37]:

$$C_f = \frac{1}{3}\frac{\epsilon_e}{1-\epsilon_e}\frac{k_1^2}{(1+k_1)^2}\frac{1}{Sh} \quad (15)$$

where $Sh = (k_f d_p)/D_m$ is the Sherwood number which is written from the Wilson and Geankoplis correlation as [18,38]:

$$Sh = \frac{1.09}{\epsilon_e^{2/3}}\nu^{1/3} \quad (16)$$

The film mass transfer coefficient of large molecules has not yet been measured. In this work, we estimate the Sherwood number for a series of non-retained polystyrene standards with different degree of exclusion from the internal pore volume of the shell of the Halo particles.

3. Experimental

3.1. Chemicals

The mobile phases were either mixtures of water and acetonitrile (20/80, 31/69, 33/67, and 37/63, v/v) or pure tetrahydrofuran. Dichloromethane ($\rho_{CH_2Cl_2} = 1.323$ g/cm^3) was used to measure the column hold-up volumes by pycnometry in combination with tetrahydrofuran ($\rho_{THF} = 0.883$ g/cm^3). These four solvents were HPLC grade from Fisher Scientific (Fair Lawn, NJ, USA). Trifluoro acetic acid (TFA) was used to set the pH buffer around 2.0 and was also purchased from Fisher Scientific. The mobile phase was filtered before use on a surfactant-free cellulose acetate filter membrane, 0.2 μm pore size (Suwannee, GA, USA). β-Lipotropin was purchased from American Peptide (Sunnyvale, CA, USA). Insulin was a generous gift from Eli Lilly (Indianapolis, IN, USA). Eleven polystyrene standards (MW = 590, 1100, 3680, 6400, 13,200, 31,600, 90,000, 171,000, 560,900, 900,000, and 1,877,000), purchased from Phenomenex (Torrance, CA, USA) were used to acquire inverse size exclusion chromatography data (ISEC). Six of them were used to measure HETP under non-retained conditions (MW = 1100, 6400, 13,200, 31,600, 90,000, and 171,000). The sample test mixture containing uracil, acetophenone, toluene, and naphthalene in pure acetonitrile, was generously offered by Phenomenex (Torrance, CA, USA).

Table 1
Physico-chemical properties of the Halo and Kinetex columns given by the manufacturer and measured in our lab.[*,$,&,%]

Neat silica	Halo 90 Å	Halo 160 Å
SEM mean particle size [μm]	2.7	2.7
$\rho = R_i/R_e$	0.63	0.63
Pore diameter [Å]	90	160
Surface area [m^2/g]	150	80
Particle size distribution ($d_{90-10\%}$)	1.13	1.13
Bonded phase analysis	**Halo-C_{18}90Å**	**Halo-C_{18}160Å**
Surface coverage [μmol/m^2]	??	??
End-capping	No	No
Particle porosity[%]	0.16	0.27
Shell porosity	0.21	0.35
Packed columns analysis		
Batch/serial number	S09004/ USHW002579	BH092206/ USKF001250
Dimension (mm × mm)	4.6 × 150	4.6 × 150
External porosity[*]	0.400	0.402
Total porosity[$]	0.498	0.563
Specific permeability[&], k_0 [cm^2]	5.9×10^{-11}	6.3×10^{-11}

[$] Measured by pycnometry (THF-CH_2Cl_2).
[*] Measured by Inverse Size Exclusion Chromatography (polystyrene standards).
[%] The particle porosity includes the volume of the solid silica core.
[&] Measured from the total back pressure data using acetonitrile/water mixtures (η = 0.54 and 1.04 cP) corrected for extra-column contributions.

3.2. Columns

The 2.7 μm Halo-C_{18} 90 Å and Halo-ES-peptide-C_{18} 160 Å columns (150 mm × 4.6 mm) were generous gifts from the column manufacturer (Advanced Material Technologies, Wilmington, DE, USA). Table 1 lists the important physico-chemical properties of these two packing materials and of the two columns used.

3.3. HPLC system, flow rate, and temperature accuracy

All the data were acquired with an Agilent 1290 Infinity HPLC system (Agilent Technology, Waldbronn, Germany) liquid chromatograph.

This instrument includes a binary pump with solvent selection valves, an auto-sampler with a 20 μL sample loop, a small volume needle seat capillary (1.2 μL), a column thermostat, a diode-array UV-detector (0.8 μL, upper sampling rate at 160 Hz), a Chemstation and its data software. New 250 mm × 85 μm inlet capillary tube (upstream the column) and 250 mm × 85 μm outlet capillary (downstream the column) were installed in order to minimize the extra-column band broadening. The 1.6 μL heat exchanger was deliberately by-passed in order to minimize the errors made in the calculation of the corrected reduced HETP, h (see below). In all experiments, the column was isolated inside the column oven. The maximum flow rate and the highest inlet pressure that can be applied to these columns are 5.0 mL/min at 800 bar and 2 mL/min at 1200 bar. Due to the narrow diameters of the connecting tubes that must be used to minimize the instrument contribution to band broadening [14], the maximum pressure drop along the column is markedly lower than the maximum operating pressure of the pump (1200 bar). The extra-column volume of our Agilent 1290 infinity system includes 115 μm I.D. connecting tubes and a UV detection cell volume of 2.4 μL. Its extra-column band broadening contribution is now nearly equivalent to that of the Acquity system from Waters [14]. Under these optimized conditions (smaller connecting tube and detection cell volumes), the extra-column contribution was significantly reduced by a factor three.

The extra-column band broadening contributions were measured by substituting the column with a zero dead volume union connector. The flow rate set to the Agilent 1290 Infinity HPLC system is true at atmospheric pressure, P^0, and ambient temperature, T = 295 K. The flow rate accuracy was checked at ambient temperature by directly collecting the mobile phase in the absence of column at 295 K and at flow rates of 0.1 mL/min, 1 mL/min, and 5.0 mL/min during 50, 25, and 10 min, respectively. The relative errors were all less than 0.3%, so we estimate the long-term accuracy of the flow-rate at 3 μL/min or better at flow rates around 1 mL/min. The laboratory temperature was controlled by an air conditioning system set at 295 K. The daily variation of the ambient temperature never exceeded ±1 °C.

3.4. Measurement of the HETP data

3.4.1. Small molecules: uracil, acetophenone, toluene, and naphthalene

The mobile phase was a mixture of water and acetonitrile (20/80, v/v). The sample volume injected was 1 μL. The concentration was kept low in order to operate in the linear range of the adsorption isotherm while keeping an acceptable signal level. An experimental test was carried out by injecting successively 1, 2, and 5 μL samples. The amount injected was considered low enough if, after normalization of all three chromatograms, the peak shapes were not distorted by either non-linear adsorption behavior or non-linear detection response. The detection wavelength was set at 254 nm. The bandwidth was fixed at 4 nm. In the presence of the column, the sampling rate was adjusted from 10 Hz (very low flow rates) to 80 Hz (high flow rates). In the absence of column (measurements of the extra-column contributions), the sampling rate was constant at 160 Hz. In all cases, the peaks were represented by at least 50 data points, e.g. the peak standard deviation was represented by at least 12 data points.

The sequence of flow rates was 0.05, 0.10, 0.20, 0.30, 0.40, 0.60, 0.80, 1.00, 1.20, 1.40, 1.60, 1.80, 2.00, 2.30, 2.60, 2.90, 3.20, and 3.50 mL/min.

The extra-column contributions to the retention volume and to the band broadening of probes were measured by replacing the chromatographic column with a zero volume union connector.

The reported experimental HETP data were corrected for the contributions of the 1290 Infinity instrument. The contribution of the extra-column band broadening is very sensitive to the nature of the eluent, through its viscosity [13]. Therefore these contributions were always measured with the same mobile phases and compounds as those that were used to measure the variance of the eluted bands. The extra-column band variance was measured according to the full integration of the best analytical fit (Gaussian-Exponentially Modified Gaussian function, 5 parameters) of the experimental band profile. Accordingly, for the sake of data accuracy, the corrected h data were systematically measured by applying the integration method for the measurement of the first (μ_1 and $\mu_{1,ex}$) and second central (μ'_2 and $\mu'_{2,ex}$) moments:

$$\mu_1 = \frac{\int_0^\infty C(t)t\,dt}{\int_0^\infty C(t)\,dt} \tag{17}$$

$$\mu'_2 = \frac{\int_0^\infty C(t)(t-\mu_1)^2\,dt}{\int_0^\infty C(t)\,dt} \tag{18}$$

The reduced column HETP h is determined using the following definition:

$$h = \frac{L}{d_p}\frac{\mu'_2 - \mu'_{2,ex}}{(\mu_1 - \mu_{1,ex})^2} \tag{19}$$

where L is the column length.

The precision of the h data is given by

$$\left|\frac{\Delta h}{h}\right| = \left|\frac{\Delta\mu_2'}{\mu_2'}\right| \left(\frac{\mu_2' + \mu_{2,ex}'}{\mu_2' - \mu_{2,ex}'}\right) + 2\left|\frac{\Delta\mu_1}{\mu_1}\right| \left(\frac{\mu_1 + \mu_{1,ex}}{\mu_1 - \mu_{1,ex}}\right) \quad (20)$$

The second and first moments of the tracer peak, μ_2' and μ_1, were measured in triplicate, first with the chromatographic column fitted to the instrument, then after replacing the column with a zero-volume connector. The relative errors made on the second and first moments were always smaller than 5 and 0.5%, respectively. Accordingly, the error made necessarily increases with decreasing solute retention e.g. when the terms in between parentheses in the right-hand-side term of Eq. (20) becomes significantly larger than one.

3.4.2. Peptide: β-lipotropin

The same method as described above for small molecules was applied, except for the eluent composition (water–acetonitrile mixture, 31/69, v/v), the addition of 0.1% TFA to this eluent, and the setting of the detector UV wavelength at 205 nm.

3.4.3. Proteins: insulin and lysozyme

The same method and experiments as described for small molecules were made, except that the eluents were mixtures of water and acetonitrile (33/67 and 37/63, v/v, for insulin and lysozyme, respectively), contained 0.1% TFA, and that the UV wavelength was set at 205 nm. The highest flow rates applied for lysozyme was only 1.4 mL/min because no acceptable signal was recorded at larger flow rates. At high flow rates, the peak width of lysozyme was too large and its height too small.

3.4.4. Polystyrene standards: MW = 1100, 6400, 13,200, 31,600, 90,000, and 171,000

The same method and experiments as described for small molecules were applied, except that the eluent was pure THF. The sequence of flow rates was 0.05, 0.10, 0.20, 0.40, 0.80, 1.20, 1.60, 2.0, 2.4, and 2.8 mL/min.

3.5. Peak parking measurements

The principle of this method was described in [39]. The flow rate was fixed at 0.4 mL/min for the small molecules (uracil, acetophenone, toluene, and naphthalene) and 0.3 mL/min for β-lipotropin and insulin. Four peak parking times were applied, e.g. 1 min, 60 min, 240 min, and 480 min. The longitudinal diffusion coefficient, B, is given by Eq. (7).

4. Results and discussion

We first discuss some important column characteristics regarding the mean particle diameter, the external porosity, the internal porosity, and the restriction for diffusion through the porous shell.

4.1. Column properties

4.1.1. Scanning electron microscopy (SEM)

Fig. 1A and B show the SEM photographs of collections of about 250 particles of Halo 90 Å and Halo-ES-peptide 160 Å, respectively. The length of the solid, thick, white segment accounts for an actual length of 10 μm. Accordingly, the manual count of a sample of 200 particles provided average particle sizes of 2.87 μm (RSD = 5.7%) and 3.02 μm (RSD = 4.2%), respectively. These two mean parti-

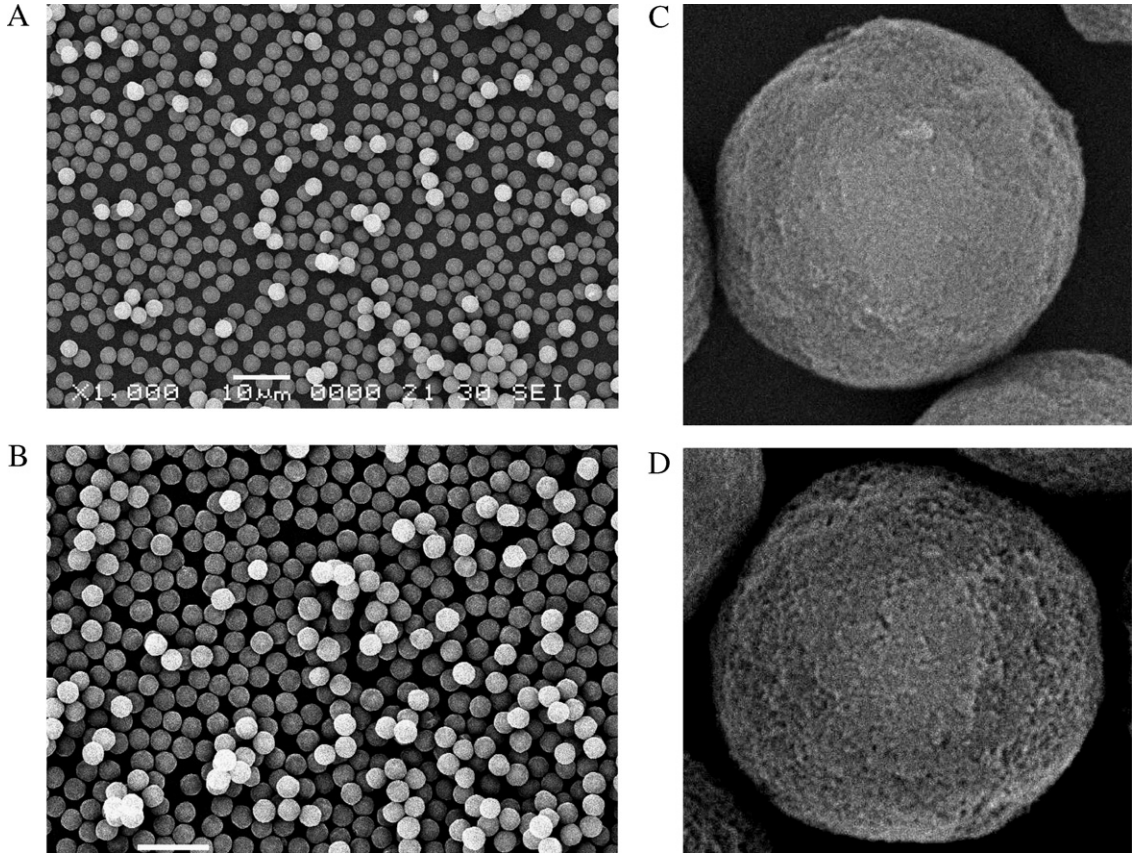

Fig. 1. SEM photographs of the 2.7 μm Halo 90 Å (A) and 2.7 μm Halo-ES-peptide 160 Å (B) particles. Note the tight size distribution of both particles (relative standard deviation 5%) and the similarity of their external shape. Zooms on one Halo standard (C) and one Halo-ES-peptide particles (D).

cle diameters are clearly larger than the commercial value of 2.7 μm given by the manufacturer. Contacted on this issue, Advanced Material Technologies confirmed that the average particle size of the particles inside the columns that they had provided to us was 2.7 μm. Most likely, the scaling of the SEM photographs was slightly in error and the accuracy of the mean particle diameter derived from the SEM photographs is doubtful. Alternative and complementary measurements will be made later.

Alternate estimates of particle sizes are provided by the Coulter counter method, which, unfortunately is biased by the influence of the particle porosity on the conductivity measurements. Because the Halo 90 Å and Halo-ES-peptide 160 Å particles differ essentially in the structure of their porous shells, the Coulter technique could not be considered in this work. A last alternative is based on the combination of measurements of the external porosities (ISEC) and permeabilities (pressure drop vs. flow rate) of these columns.

4.1.2. Inverse size exclusion chromatography (ISEC)

The experimental ISEC plots of the two Halo columns are shown in Fig. 2A and B, respectively. Solutions of 11 polystyrene standards in pure tetrahydrofuran were injected (1 μL at 1 g/L) at a flow rate of 0.4 mL/min. The data were corrected for the extra-column time which represents only in between 0.6% (MW = 590) and 1.2% (MW = 1,870,000) of the elution time of the polymer. Thus, the accuracy of the elution times is better than 1% and the precision better than 0.5%. The sizes of the lighter polymers to be excluded from the internal porous volumes of the shell particles are 95 Å (MW = 31,600) and 170 Å (MW = 90,000) for the Halo 90 Å and Halo 160 Å, respectively. Extrapolation of the excluded branches of the ISEC plots (see the bottom dotted line) to a molecular weight of zero gives practically the same value of external porosity (ϵ_e = 0.400 and 0.402). Both columns are packed very similarly. They differ from their respective internal shell porosity accessible to pure THF, $\epsilon_{p,shell}$ = 0.358 and 0.217, assuming the same ratio ρ = (1.7/2.7) = 0.63 for both particles.

ISEC data provides useful information regarding the transport of sample molecules through the porous shell of the particles. Table 2 lists the values of the accessible shell porosity, internal obstructive factor [39],$\gamma_{p,shell}$, and hindrance diffusion factor [40], $F(\lambda_m)$, for all the compounds tested in this work. The pore diffusivity of large molecules is obviously less restricted through the Halo-C_{18} 160 Å particles than through the Halo-C_{18} 90 Å particles. The pore diffusivity is written [36]:

$$D_{pores} = \epsilon_{p,shell}\gamma_{p,shell}F(\lambda_m) \quad (21)$$

where $\gamma_{p,shell}$ is derived from experimental data obtained with fully porous particles [39]:

$$\gamma_{p,shell} = \frac{1}{(1.8 - \epsilon_{p,shell})^2} \quad (22)$$

and $F(\lambda_m)$ can be estimated from the Renkin correlation [40]:

$$F(\lambda_m) = (1-\lambda_m)^2(1 - 2.1044\lambda_m + 2.089\lambda_m^3 - 0.948\lambda_m^5) \quad (23)$$

where λ_m is the ratio of the sample size to the mean pore diameter (see Table 2).

These data suggest that the pore diffusivity of non-retained small molecules (size <5 Å) is about twice larger through the shell of Halo 160 Å particles than through those of Halo 90 Å particles. The same ratio is increased to 3 and 6 if we consider the larger molecules of β-lipotropin (12 Å) and insulin (32 Å). In the same time, surface diffusion plays an important role under retained conditions in RPLC and accounts for most of the sample diffusivity through particles [41,42].

4.1.3. Permeability data

Fig. 3A and B show the plots of the column pressure drop (after correction for the extra-column back pressure) *versus* the flow rate

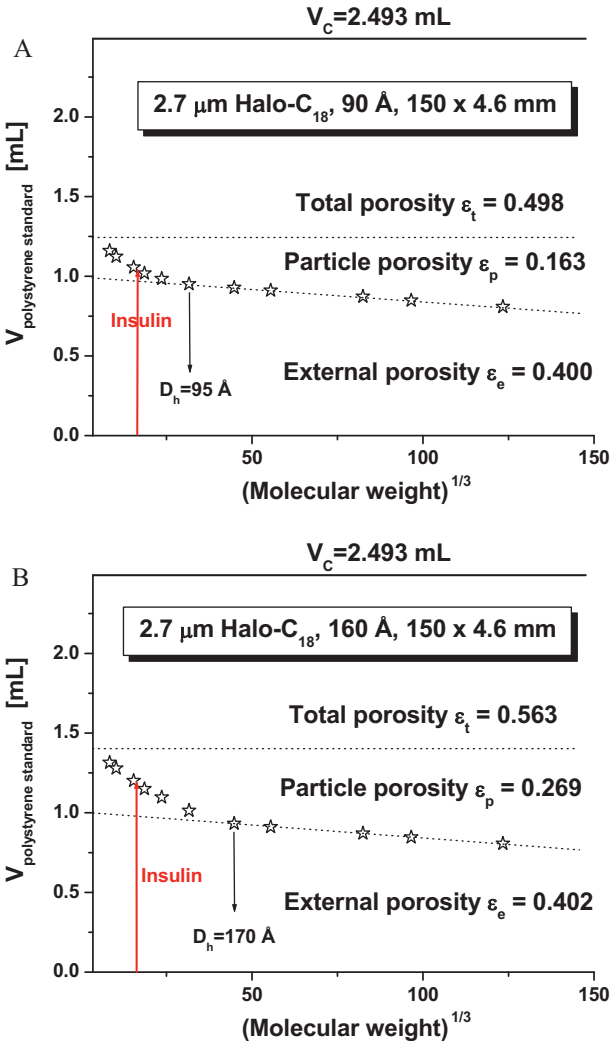

Fig. 2. ISEC measurements. Eluent: pure tetrahydrofuran. Flow rate: 0.4 mL/min. T = 295 K. Plots of the elution volumes of 11 polystyrene standards *versus* the cubic root of their average molecular weights ($MW^{1/3}$). Two 4.6 mm × 150 mm columns packed with two brands of particles were studied. (A) Core-shell 2.7 μm Halo-C_{18} 90 Å. (B) Core-shell Halo-ES-peptide-C_{18} 160 Å. The external porosities, ϵ_e, were extrapolated at MW = 0 from the excluded ISEC branch of each plot (bottom and non-horizontal dotted lines). The upper solid horizontal lines stand for the total column volume (V_c). The dotted horizontal lines stand for the total porosities (ϵ_t). The distance between these two lines measures the internal volume of the particles (ϵ_p). Note the smaller particle porosity of the standard Halo 90 Å particles.

applied to both columns for two different mixtures of water and acetonitrile, (20/80 and 69/31, v/v, respectively). The specific permeabilities, k_0, of the columns were derived from the slope of these plots [35]:

$$k_0 = \frac{\eta L}{\pi R_c^2(\Delta P/F_v)} \quad (24)$$

where L is the column length (15 cm) and R_c is the column inner radius (0.23 cm). The viscosities of the two eluents are η = 0.54 and 1.04 cP. The experimental data demonstrate that the Halo-ES-peptide column is slightly less permeable than the standard (90 Å) Halo column (−5 to −10%). The average specific permeability of the Halo-ES-peptide column was found to be 5.9×10^{-11} cm^2. That of the Halo 90 Å column was 6.3×10^{-11} cm^2. A different degree of frit clogging in these two columns could potentially explain these differences.

If we introduce d_p = 3.02 μm, the particle size of the Halo-ES-peptide particles given by the SEM photograph in Fig. 1B, into the

Table 2
Shell porosities accessible to the sample molecules ($\varepsilon_{p,shell}$), ratio of the sample radius to the average pore size radius (λ_m), hindrance diffusion factors ($F(\lambda_m)$), and internal obstructive factor ($\gamma_{p,shell}$) of all the sample molecules used in this work with their molecular size (D_h).

Sample	Mobile phase	$\varepsilon_{p,shell}$		$\gamma_{p,shell}$		λ_m		$F(\lambda_m)$	
		Halo 90 Å	Halo 160 Å	Halo 90 Å	Halo 160 Å	Halo 90 Å	Halo 160 Å	Halo 90 Å	Halo 160 Å
Small molecules									
Uracil, D_h < 5 Å	80% CH_3CN	0.217	0.358	0.40	0.48	<0.06	<0.04	>0.88	>0.93
Acetophenone, D_h < 5 Å	80% CH_3CN	0.217	0.358	0.40	0.48	<0.06	<0.04	>0.88	>0.93
Toluene, D_h < 5 Å	80% CH_3CN	0.217	0.358	0.40	0.48	<0.06	<0.04	>0.88	>0.93
Naphthalene, D_h < 5 Å	80% CH_3CN	0.217	0.358	0.40	0.48	<0.06	<0.04	>0.88	>0.93
Peptide									
β-Lipotropin, D_h = 12 Å	31% CH_3CN	0.138	0.269	0.36	0.43	0.133	0.075	0.71	0.84
Proteins									
Insulin, D_h = 32 Å	33% CH_3CN	0.065	0.184	0.33	0.38	0.356	0.200	0.30	0.57
Lyzozyme, D_h = 42 Å	37% CH_3CN	0.034	0.146	0.32	0.37	0.467	0.262	0.16	0.45
Polymers									
Polystyrene, MW = 1100, D_h = 14 Å	100% THF	0.128	0.262	0.36	0.42	0.156	0.087	0.66	0.81
Polystyrene, MW = 6400, D_h = 38 Å	100% THF	0.045	0.159	0.32	0.37	0.422	0.237	0.21	0.49
Polystyrene, MW = 13,200, D_h = 58 Å	100% THF	0.022	0.119	0.32	0.35	0.644	0.362	0.06	0.29
Polystyrene, MW = 31,600, D_h = 95 Å	100% THF	0.003	0.056	0.31	0.33	1.000	0.594	0.00	0.08
Polystyrene, MW = 90,000, D_h = 171 Å	100% THF	Excluded	0.002	Excluded	0.31	Excluded	1.000	Excluded	0.00
Polystyrene, MW = 171,000, D_h = 245 Å	100% THF	Excluded	Excluded	Excluded	Excluded	Excluded	Excluded	Excluded	Excluded

Kozeny-Carman constant:

$$k_0 = \frac{\epsilon_e^3 d_p^2}{K_c(1-\epsilon_e)^2} \quad (25)$$

we obtain a value of 290, too large compared to the standard value of 180, which suggests that the particle size was overestimated. However, the permeability actually measured would correspond to a particle size of 2.4 μm if the Kozeny-Carman constant is 180, which, in turn, is an underestimate of the particle size of the Halo particles. Therefore, we conclude that either the pressure drop measured is higher than expected (due to frit clogging, with $\Delta P = \Delta P_{bed} + \Delta P_{frit}$) or that the Kozeny-Carman constant of the Halo columns is larger than 180. Note that if frit clogging were the sole responsible and assuming that the SEM data were true with K_c = 180, ΔP_{frit} would account for 40% of the overall pressure drop, which seems to be excessive. Yet, we ignore the extent of frit clogging in HPLC columns and its contribution to the overall pressure drop and we cannot make any unambiguous conclusion at this time. Accordingly, we consider that permeability data are not reliable to estimate the particle sizes and that the SEM data are inconsistent with the manufaturer's data. In the next sections, we adopted the values given by the manufacturer for each column and considered that the mean particle diameter of both the Halo-ES-peptide and the Halo standard particles was 2.70 μm.

4.2. Van Deemter plots

From the HETP data, we derived the characteristics of the mass transfer of a few low molecular weight compounds (uracil, acetophenone, toluene, and naphthalene), of one peptide (β-lipotropin), of two proteins (insulin and lysozyme), and of six polystyrene standards (MW = 1100, 6400, 13,200, 31,600, 90,000, and 171,000). In each case, we compare the reduced HETP and investigate the difference between the overall C term of the Halo and the Halo-ES-peptide columns. Peak parking measurements were performed in order to estimate the particle diffusivity and the trans-particle mass transfer resistance coefficient, C_p [16]. The difference between the experimental C and the semi-empirical C_p coefficients informs on the importance of the external film mass transfer in the kinetic behavior of the Halo columns at high linear velocities. It should provide an unambiguous answer and clear physical explanations regarding the possible difference in the kinetic behavior of the first generation of Halo columns (pore size 90 Å) and the new Halo-ES-peptide columns (pore size 160 Å).

4.2.1. Small molecules

Fig. 4A–D show the reduced HETP's of uracil, acetophenone, toluene, and naphthalene, respectively. Through proper selection of the eluent composition, the retention factors were kept relatively small (<1.5) in order to limit the possible influence of heat friction at high flow rates on the experimental HETP. Therefore, the C term measured is controlled only by the external film mass transfer resistance and the shell diffusivity. Small molecules have molecular size (<5 Å) comparable to that of the eluent molecules and have access to the whole mesopore volume. Table 3 lists the values of the longitudinal diffusion coefficient, B (peak parking experiments), and C_p (peak parking experiments combined with either of the two diffusion models in the packed bed) for each probe molecule. Table 4 compares the effective diffusivity, D_{shell}, of the compounds through the shells of both Halo particles.

Three main comments can be made at this points:

- The longitudinal diffusion coefficient, B, is slightly larger with the new Halo-ES-peptide column than with the standard Halo col-

Table 3
Results for the measurement at room temperature (T = 295 K) of the zone retention factor k_1, the B (peak parking experiments) and the C_p (peak parking + parallel diffusion model and EMT model) coefficients in their general reduced HETP equation for five different samples used in this work.

Sample	Mobile phase	k_1		B		C_p	
		Halo 90 Å	Halo 160 Å	Halo 90 Å	Halo 160 Å	Halo 90 Å	Halo 160 Å
Uracil	80% CH_3CN	0.25	0.40	1.69	1.95	0.003	0.004
Acetophenone	80% CH_3CN	0.61	0.68	2.66	2.96	0.004	0.003
Toluene	80% CH_3CN	1.35	1.09	3.57	3.67	0.005	0.004
Naphthalene	80% CH_3CN	1.61	1.25	3.35	3.55	0.006	0.005
β-Lipotropin	31% CH_3CN	0.98	1.35	2.26	3.13	0.009	0.004
Insulin	33% CH_3CN	0.52	1.33	1.15	1.43	0.021	0.012

Table 4
Results for the measurement (peak parking experiments) at room temperature (T = 295 K) of the shell diffusivities according to the parallel diffusion model ($D_{shell,parallel}$) and the effective medium theory ($D_{shell,EMT}$).

Sample	Mobile phase	$D_{shell,parallel}$ [cm^2/s]		$D_{shell,EMT}$ [cm^2/s]	
		Halo 90 Å	Halo 160 Å	Halo 90 Å	Halo 160 Å
Uracil	80% CH_3CN	2.49×10^{-6}	3.85×10^{-6}	1.93×10^{-6}	2.64×10^{-6}
Acetophenone	80% CH_3CN	9.01×10^{-6}	1.10×10^{-5}	5.97×10^{-6}	7.37×10^{-6}
Toluene	80% CH_3CN	1.62×10^{-5}	1.70×10^{-5}	1.15×10^{-5}	1.21×10^{-6}
Naphthalene	80% CH_3CN	1.27×10^{-5}	1.40×10^{-5}	8.79×10^{-6}	9.85×10^{-6}
β-Lipotropin	31% CH_3CN	1.18×10^{-6}	3.06×10^{-6}	7.92×10^{-7}	2.22×10^{-6}
Insulin	33% CH_3CN	– [a]	3.65×10^{-7}	1.08×10^{-7}	2.85×10^{-7}

[a] The value obtained was negative and made no sense based on the parallel diffusion model.

umn. This is consistent with the larger internal volume of these new shell particles and the less restricted molecular diffusion within larger mesopores (see Table 2). The results of the peak parking method show that this difference is marginal (+2%) for the most retained compounds, due to the important role played by surface diffusion and the specific surface area being larger for Halo 90 Å particles (150 *versus* 80 m^2/g). The difference is maximum but moderate with the least retained compounds (+10-15%) for which surface diffusion is nearly negligible. The diffusion coefficient, D_{shell}, is only 5–40% larger in the shells of Halo-ES-peptide 160 Å than in those of Halo 90 Å particles.

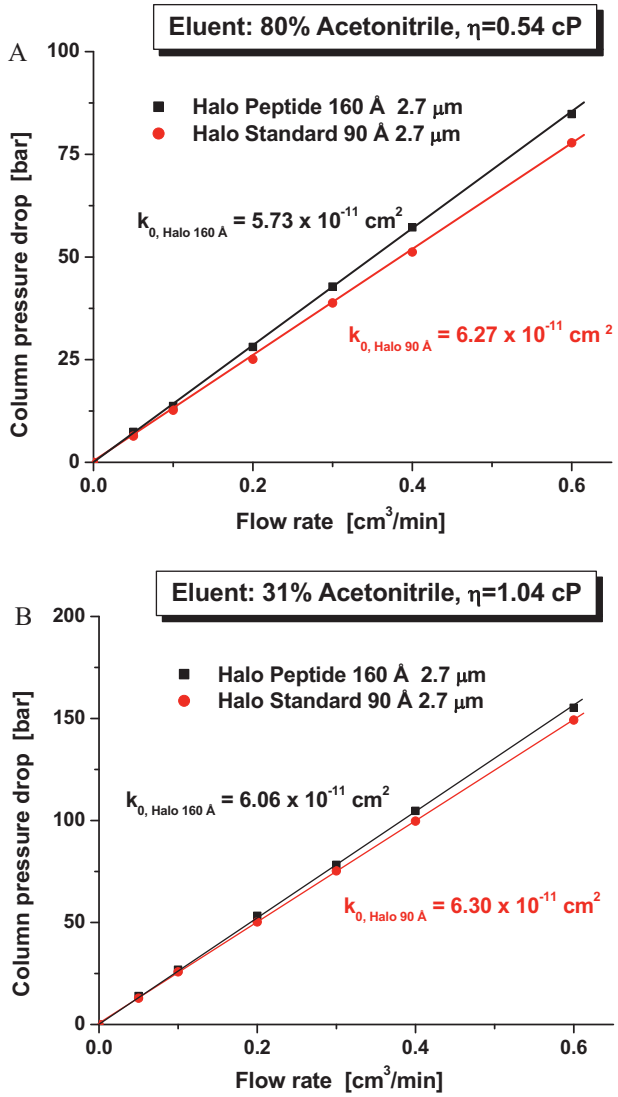

Fig. 3. Plots of the column pressure drops of Halo 90 Å (full circles) and Halo-ES-peptide 160 Å (full squares) columns after correction for the system (optimized Agilent 1290 Infinity) pressure drop in the low flow rate range. Two different mixtures of acetonitrile and water we used as the mobile phase: (A) 80/20, v/v; (B) 31/69, v/v. Note the comparable permeability of the two Halo columns. The values of the respective specific permeabilities (in cm^2) are indicated in the graphs.

- The eddy diffusion coefficient, A, is smaller with the new Halo-ES-peptide column (−25%). This result is not explained by a higher degree of bed homogeneity because the external porosity of this bed (ϵ_e = 0.40), the width of the particle size distribution (RSD ≃ 5%), and the external shape of the shell particles (see SEM pictures in Fig. 1A and B) are most similar for both columns. More likely, it confirms a recent observation made with porous and non-porous particles [43,44,34], demonstrating that the diffusivity of the probe compound across the porous particles contributes to decrease the eddy diffusion coefficient. Indeed, sample diffusivity through the porous shells is faster with Halo 160 Å particles than with Halo 90 Å particles (see results in Table 3 from the peak parking method), the difference in the A terms observed is consistent with this explanation. Fig. 5A–D show the HETP data corrected by subtraction of the longitudinal diffusion term (measured by the peak parking method, Eq. (7)), the trans-particle mass transfer resistance term (estimated by combining the peak parking method, the parallel or effective medium theory diffusion model, Eq. (14)), and the external film mass transfer resistance (Wilson and Geankoplis correlation, Eq. (15)). All graphs clearly show the smaller A term of the Halo-ES-peptide column for all small molecules.
- The measured overall C coefficient is smaller for the Halo-ES-peptide column than for the Halo 90 Å one. The decrease is about 35% (0.022 *versus* 0.042, 0.011 *versus* 0.015, 0.008 *versus* 0.012, and 0.015 *versus* 0.022 for uracil, acetophenone, toluene, and naphthalene, respectively). Note that these overall C coefficient are significantly larger than the trans-particle C_p coefficient ($0.003 < C_p < 0.006$, see Table 3) which is not the only source of solid–liquid mass transfer resistance. Additionally, the C_p coefficients are similar for both columns (0.003 *versus* 0.004, 0.004 *versus* 0.003, 0.005 *versus* 0.004, and 0.006 *versus* 0.005 for uracil, acetophenone, toluene, and naphthalene, respectively). Thus, the larger C term observed for the standard Halo 90Å column is due to its higher external film mass transfer resistance because the access to the mesoporous volume is more difficult when the shell porosity is low. This assumption will be checked in the next section with larger molecules, which are partially excluded from the mesopore volume.

Table 4 lists the shell diffusivities of the non-retained compound, uracil. They are about 1.5 times larger through the Halo 160 Å particles than through the Halo 90 Å. It is noteworthy that, as the retention factor increases, this ratio continuously decreases from 1.46, 1.22, 1.05, and 1.10 because the contribution of surface

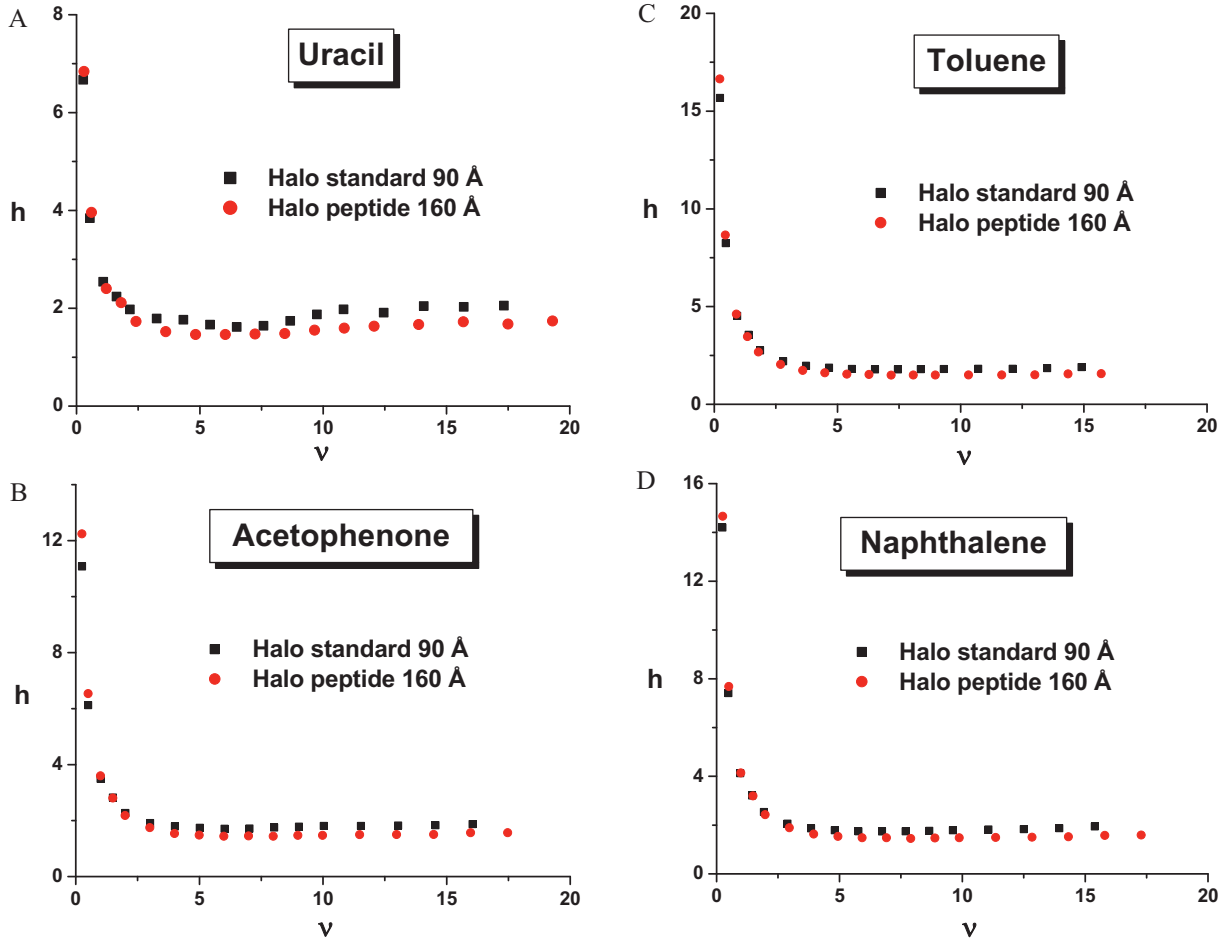

Fig. 4. Plots of the reduced HETPs of small molecules measured on the Halo 90 Å (full squares) and Halo-ES-peptide 160 Å (full circles) columns. T = 295 K. Eluent: acetonitrile–water (80/20, v/v): (A) uracil; (B) acetophenone; (C) toluene; (D) naphthalene. Note the flat C branch and the smaller eddy diffusion coefficient A with the Halo-ES-peptide column.

diffusion to the shell diffusivity compensates for the small pore diffusivity of the Halo 90 Å particles.

4.2.2. Peptide molecule

The peptide β-lipotropin was chosen because it contains no ionizable amino group in the side-chains of its eight amino-acids (Ala-Ala-Ala-Tyr-Gly-Gly-Phe-Leu). Its peak should not tail significantly much at pH = 2.0 in the presence of 0.1% TFA in a mixture of water and acetonitrile (31/69, v/v) due to secondary interactions between the peptide and the stationary phase. The accuracy and precision of the reduced HETP will then not be affected by either a noisy signal (too dilute a sample) or an asymmetrical peak (thermodynamic tailing). The average molecular diameter of this peptide is about 12 Å and its molecular weight is 769 Da. This diameter was calculated in pure water, based on the known sequence of amino acids of this peptide. The bulk molecular diffusion coefficient of β-lipotropin is equal to 2.6×10^{-6} cm^2/s.

Fig. 6A shows the corresponding reduced HETP plots of β-lipotropin on both Halo columns. The minimum reduced HETP, h_{min}, is shifted toward a higher reduced linear velocity with the Halo 160 Å column (ν_{min} = 8 *versus* ν_{min} = 4 for Halo 90 Å). The minimum reduced HETP also decreases from 1.8 to 1.4. The difference in the kinetic behavior of the two Halo columns is directly due to a smaller C term and a sightly larger B term for the Halo-ES-peptide column. Table 3 lists the value of the B coefficient derived from the peak parking measurements. It increases from 2.26 (Halo 90 Å) to 3.13 (160 Å). Fig. 6B illustrates the larger B term measured with the Halo-ES-peptide column at a low flow rate of 0.05 mL/min. The efficiency of the 15 cm long Halo-ES-peptide column is 20% smaller than that of the standard Halo column despite its lower A term. On the other hand, Fig. 6C illustrates that, at high flow rates (2.8 mL/min), the solid–liquid mass transfer resistance of the new Halo 160 Å shell particles is smaller than the one of the standard Halo 90 Å. At this high velocity, the efficiency of the Halo-ES-peptide column is 60% higher than that of the standard Halo column. The relative decrease of the C term of β-lipotropin from the Halo-C_{18} 90 Å to the Halo-C_{18} 160 Å column is directly correlated to the relative increase of the accessible porosity of the shell (0.14–0.27).

A most striking result is that the average C term of β-lipotropin on both Halo columns is larger than this term for small molecules. The average C coefficient of toluene, which has about the same retention factor as β-lipotropin, is 0.010 (0.012 and 0.008). The average C coefficient of β-lipotropin is 0.049 (0.062 and 0.036). This large difference cannot be attributed to the difference in the particle diffusivity (parameter $\Omega = D_{shell}/D_m$), according to the semi-empirical C_p coefficients given in Table 3 (0.009 and 0.004). In conclusion, the slow solid–liquid mass transfer observed with β-lipotropin is explained by an external film mass transfer resistance stronger than that experienced by small molecules. Again, the porosity of both Halo shells accessible to the peptide molecules is smaller (0.14 and 0.27) than that accessible to small molecules (0.22 and 0.36). This confirms the initial interpretation made in the previous section with small molecules. Next, we extend this C term theory to even larger and more excluded molecules, insulin and lysozyme.

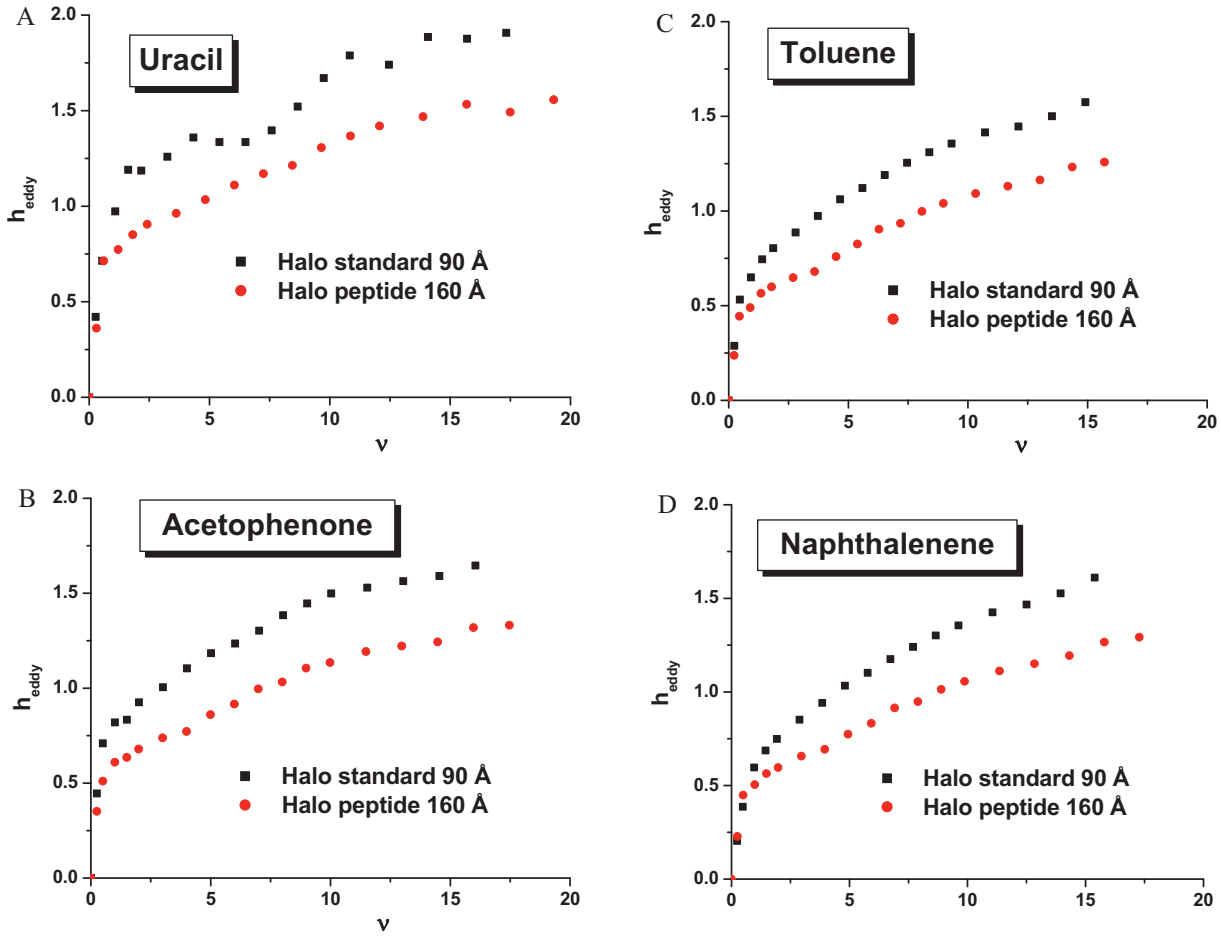

Fig. 5. Same as in Fig. 4, except the plot of eddy diffusion coefficient A, measured after subtraction of the longitudinal diffusion term B/ν, the trans-particle mass transfer coefficient, C_p, and the external film mass transfer resistance term (Wilson and Geankoplis) to the reduced HETP data. Confirmation of the lower A term of the new Halo-ES-peptide column with respect to that of the standard Halo column.

4.2.3. Proteins: insulin and lysozyme

The molecular weights of insulin and lysozyme are 5.8 and 14.7 kDa, respectively. Their molecular sizes are 32 and 42 Å, therefore, they are both significantly excluded from the internal volume of the porous shells (see Table 2). The actual shell porosities accessible to insulin are 0.18 (Halo 160 Å) and 0.07 (Halo 90 Å). They are 0.15 and 0.03 for the larger protein lysozyme. The content of acetonitrile was adjusted to 33% and 37% to observe moderate retention factors and keep a high signal-to-noise ratio. The bulk molecular diffusion coefficients of inusulin and lysozyme are 1.6×10^{-6} cm^2/s and 9.6×10^{-7} cm^2/s, respectively.

4.2.3.1. Insulin. Fig. 7A shows the reduced HETP's of the Halo columns and compares them to that of the Kinetex 100 Å column. Impressively, the solid–liquid mass transfer on the new Halo-ES-peptide column is 3.5 times faster than that measured for the standard Halo 90 Å column, the overall C term (derived from HETP data for $10 < \nu < 100$) being 0.295 and 0.084, respectively. Note that these C terms are clearly larger than the C_p terms, 0.021 and 0.012, measured with the peak parking method. Again, consistent with the observations made for small molecules and the peptide, the significant decrease of the C term is explained by a reduction of the external film mass transfer coefficient. Increasing the shell porosity accessible to insulin (0.18 *versus* 0.07) accelerates the mass transfer through the stationary film surrounding the shell particles. Fig. 7A demonstrates that it is not the average mesopore size itself but the shell porosity of the C_{18}-derivatized material that controls the mass transfer of insulin. Indeed, the mesopore size of the Kinetex column is only 100 Å (similar to that of the standard Halo 90 Å column) but the porosity of its shell particles is large (0.32 [15]) and comparable to that of the Halo-ES-peptide column (0.36), which explains the flat C branch of this column.

The C coefficient of insulin on the Halo 90 Å column is 5 and 60 times larger than those of the peptide (β-lipotropin) and of the small molecules, respectively. The trans-particle mass transfer resistance coefficient, C_p, of insulin is 0.022, accounting for nearly 8% of the overall C coefficient derived from the HETP data. As suggested in the previous sections, the large absolute value of the C coefficient of insulin cannot be physically explained by the sole, slow diffusivity of insulin in the porous shell (D_{shell} = 1.08×10^{-7} cm^2/s). The external film mass transfer resistance controls more than 90% of the solid–liquid mass transfer resistance of proteins. As far as the Halo 160 Å column is concerned, the solid–liquid C coefficient of insulin is only 2.5 and 20 times larger than those of β-lipotropin and toluene, respectively. Note that the C_p coefficient is 0.021 (D_{shell} = 2.85×10^{-7} cm^2/s), accounting for up to 15% of the solid–liquid mass transfer.

For the sake of illustrating the enhanced performance of the Halo-ES-peptide column compared to that of the standard Halo column, Fig. 7B shows the chromatograms of insulin at a flow rate of 2.8 mL/min on both columns. Despite a larger elution time, the half-height peak width of insulin eluted on the new Halo column is thinner than that measured with the standard Halo column.

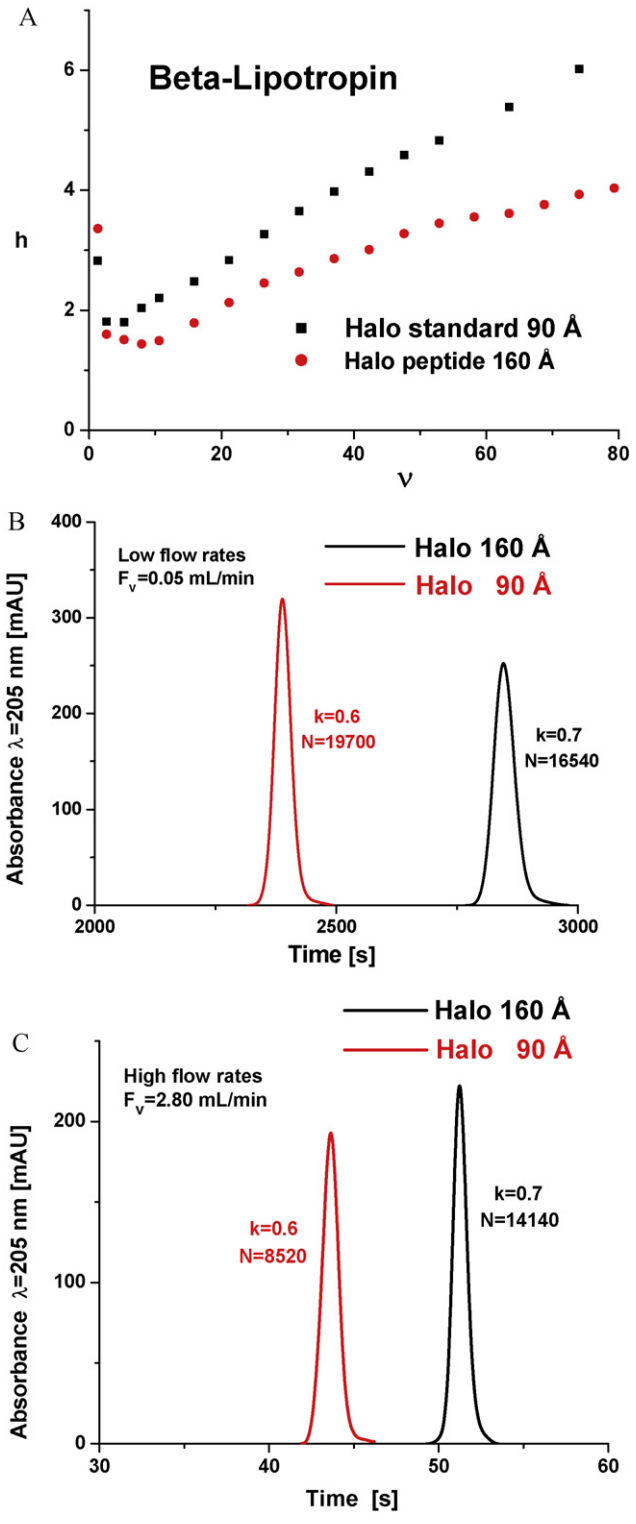

Fig. 6. (A) Plots of the reduced HETPs of β-lipotropin on the Halo 90 Å (full squares) and Halo-ES-peptide 160 Å (full circles) columns. T = 295 K. Eluent: acetonitrile–water–TFA (31/69/0.1, v/v/v). Corresponding chromatograms recorded at 0.05 mL/min (B) and 2.80 mL/min (C).

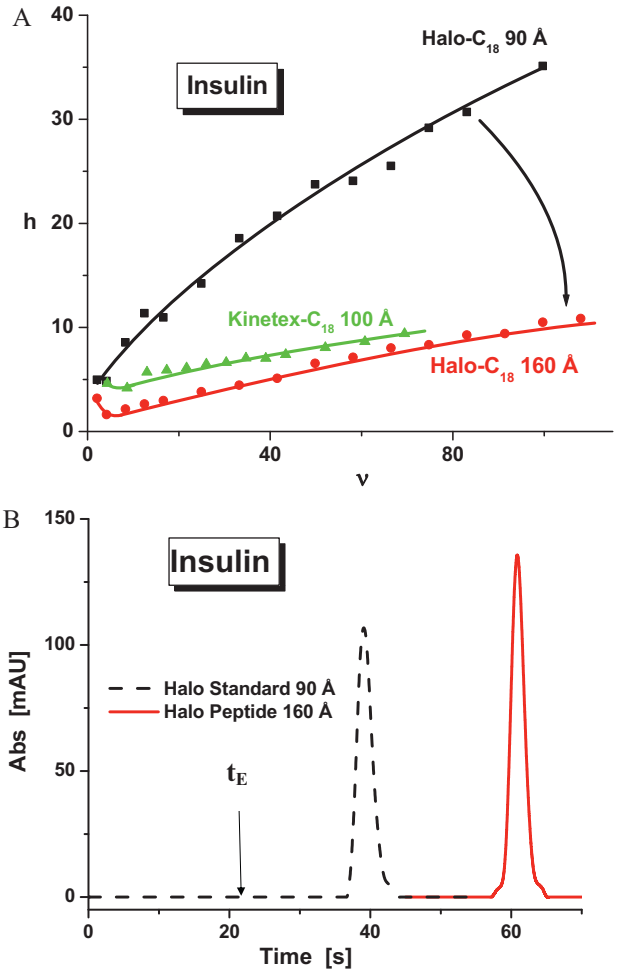

Fig. 7. (A) Plots of the reduced HETPs of insulin on Halo 90 Å (full squares), Halo-ES-peptide 160 Å (full circles), and Kinetex 100 Å columns. T = 295 K. Eluent: acetonitrile–water–TFA (33/67/0.1, v/v/v). (B) Chromatograms recorded on both Halo columns at a flow rate of 2.80 mL/min. The triangles represent the same data measured on a 100 mm × 4.6 mm 2.6 μm Kinetex column. See more details in [15].

4.2.3.2. Lysozyme. The reduced HETP of lysozyme can be measured only for the Halo 160 Å column. Fig. 8A and B show the chromatograms of lysozyme on both columns at flow rates of 0.4 and 1.0 mL/min, respectively. The peaks of lysozyme tail strongly on the standard Halo column while they are nearly symmetrical on the new Halo column. We note that lysozyme has very limited access to the internal volume of the Halo 90 Å particles ($\epsilon_{p,shell}$ = 0.034). Fig. 8C shows the reduced HETP data of lysozyme measured on the Halo-ES-peptide column. The overall solid–liquid C coefficient is 0.639 (0.295 for insulin, 0.036 for β-lipotropin, and 0.008 for toluene). The volume fraction of the shells accessible to lysozyme is 0.15 (0.18 for insulin, and 0.27 for β-lipotropin). This continuous increase of the C term from the peptide, to insulin, and to lysozyme makes sense on the basis of solid–liquid mass transfer resistance terms governed by the external film mass transfer, which becomes slower with decreasing access to the internal volume.

In the next section, we investigate further the mass transfer mechanism of large molecules in Halo columns by selecting as probe compounds, a series of non-retained and excluded polystyrene standards. The overall solid–liquid C coefficient is measured, the C_p coefficient is estimated from Eq. (14). The influence of the external film mass transfer is obtained by subtracting the latter from the former coefficient.

4.2.4. Polystyrene standards: MW = 1100, 6400, 13,200, 31,600, 90,000, and 171,000

These six polystyrene standards have hydrodynamic diameters of 14.2, 38.4, 57.8, 94.5, 170.6, and 245 Å, respectively. Their bulk molecular diffusion coefficients in pure THF are 6.64×10^{-6}, 2.46×10^{-6}, 1.64×10^{-6}, 1.00×10^{-6}, 5.54×10^{-7}, and

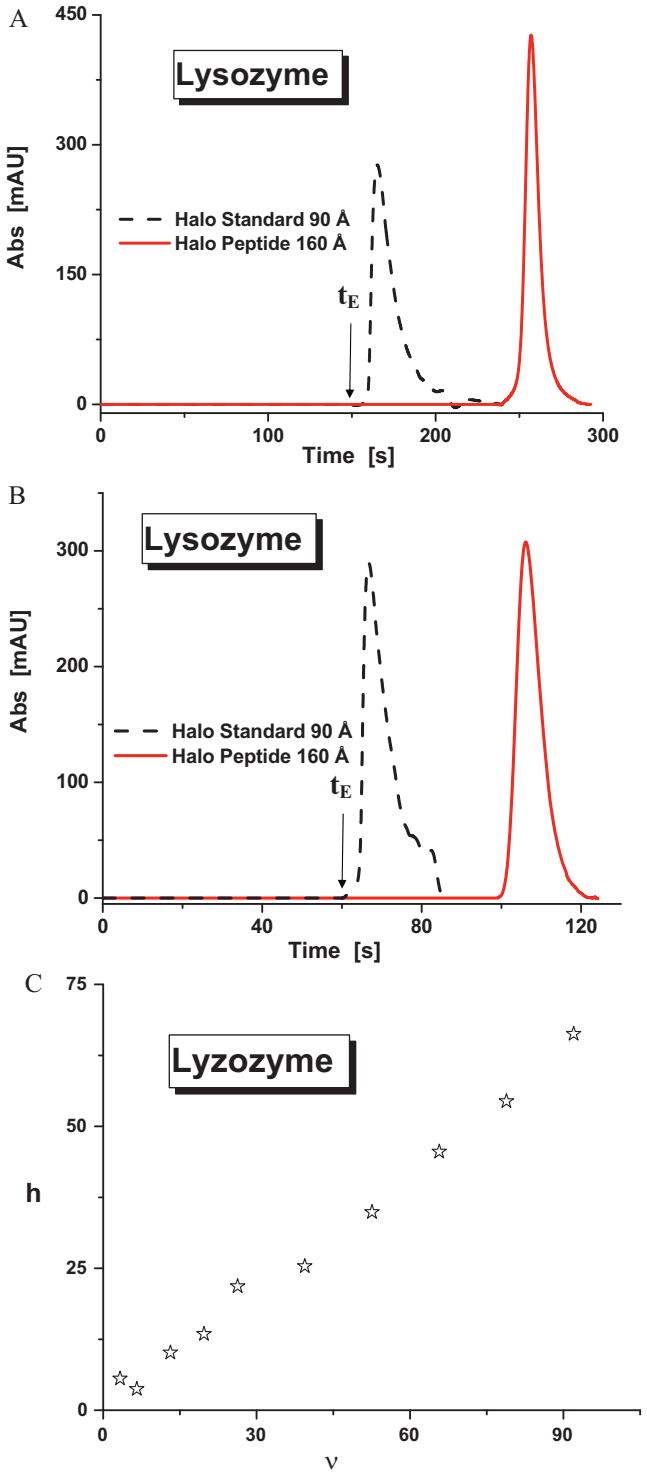

Fig. 8. Chromatograms of lysozyme on both Halo columns. T = 295 K. Eluent: acetonitrile–water–TFA (33/67/0.1, v/v/v): (A) flow rate: 0.4 mL/min; (B) flow rate: 1.0 mL/min. Note the strong exclusion and the enhanced peak tailing of lysozyme with the Halo 90 Å column. (C) Reduced HETP data of lysozyme with the Halo 160 Å column.

3.86×10^{-7} cm^2/s [22]. The size of the first standard is similar of that of β-lipotropin (12 Å). That of the second one is comparable to those of insulin (32 Å) and lysozyme (42 Å). The third one has a size comparable to that of larger proteins (40 kDa). The fourth one is excluded from the mesopore volume of the Halo 90 Å particle (see Fig. 2A) and has access to about 6% of the internal shell volume of the Halo 160 Å particles. The fifth one is excluded from the mesopore volume of the Halo-ES-peptide column (see Fig. 2B). Finally, the sixth polystyrene standard is completely excluded from the internal volume of both shells.

No polystyrene standard is retained on the stationary phase and their degree of exclusion increases with increasing molecular weight. The volume fraction of the internal volume of the shell accessible to these polymers, $\epsilon_{p,shell}$ (Table 2), decreases from 26.2, 15.9, 11.9, 5.6, 0.2, to 0.0% on Halo 160 Å particles. These volume fractions are respectively 12.8, 4.5, 2.2, 0.3, 0.0, and 0.0% on the Halo 90 Å particles. The hindrance diffusion factors, $F(\lambda_m)$ are 0.66, 0.21, 0.06, 0, 0, and 0 on the standard Halo packing material but 0.81, 0.49, 0.29, 0.08, 0, and 0 on the new Halo-ES-peptide 160 Å particles. Because no polystyrene standard is retained, their effective diffusivity through the porous shell is directly given by Eq. (21).

The theoretical C_p term is obtained for non-retained compounds and shell particles from Eq. (14) with the zone retention factor k_1 written as:

$$k_1 = \frac{1-\epsilon_e}{\epsilon_e}\epsilon_{p,shell}(1-\rho^3) \tag{26}$$

Accordingly, the trans-particle C_p coefficients are estimated to 0.007 (MW = 1100), 0.010 (MW = 6400), and 0.019 (MW = 13,200) on the Halo 90 Å column. They are equal to 0.008 (MW = 1100), 0.010 (MW = 6400), and 0.015 (MW = 13,200), and 0.032 (MW = 31,600) on the Halo 160 Å.

Fig. 9A–F shows the corresponding reduced HETP plots. As expected, the HETPs in Fig. 9E-F are very similar because the polystyrene standards are excluded from the internal volume of both Halo particles. The HETPs in Fig. 9A show a very flat C branch because this small polymer has access to a large fraction of the pore volume. The most noticeable differences are observed for polymers with molecular size between 30 and 100 Å (Fig. 9B-D) when the ratio of the accessible particle porosities is the largest (see Table 2).

The overall experimental C coefficients are 0.055 (MW = 1100), 0.096 (MW = 6400), 0.145 (MW = 13,200), and 0.254 (MW = 31,600) on the Halo 160 Å column. They are about one order of magnitude larger than the C_p coefficients. Those of the Halo 90 Å column are even larger at 0.145 (MW = 1100), 0.340 (MW = 6400), and 0.540 (MW = 13,200). Again, these C values clearly exceed the semi-empirical C_p values. In conclusion, the solid–liquid mass transfer resistance of large molecules through both Halo columns is mostly (∼ 90%) governed by the external film mass transfer resistance. The contribution of the polymer diffusivity through the shell particles happened to be negligible with 2.7 μm shell particles. These experiments demonstrate that the Sherwood number, Sh, of large molecules strongly depends on the porosity of the particles. The Sherwood number is measured as [37,43]:

$$Sh = \frac{k_f d_p}{D_m} = \frac{1}{3}\frac{\epsilon_e}{1-\epsilon_e}\left(\frac{k_1}{1+k_1}\right)^2\frac{1}{C-C_p} \tag{27}$$

Fig. 10 shows that the logarithm of the dimensionless Sherwood number of the polystyrene standards (in pure THF, with 2.7 μm Halo particles) increases linearly with increasing logarithm of the porosity of the shell particles accessible to the polymer ($Sh \propto \epsilon_{p,shell}^{2.75}$). Furthermore, the data measured with both Halo 90 Å and Halo 160 Å columns are on the same straight line. This proves that the average pore size does not directly control the external film mass transfer resistance nor the C term of the columns. A better accessibility of the pores via larger openings would reduce the C term by reducing the resistance to external film mass transfer. In other words, the larger the fraction of the external surface area of the particle that is open to the bulk eluent, the faster the transfer of the sample through the stagnant film of eluent surrounding the Halo particles. This conclusion is consistent with the experimental C branch of insulin (see Fig. 7A) measured for the Halo 90 Å

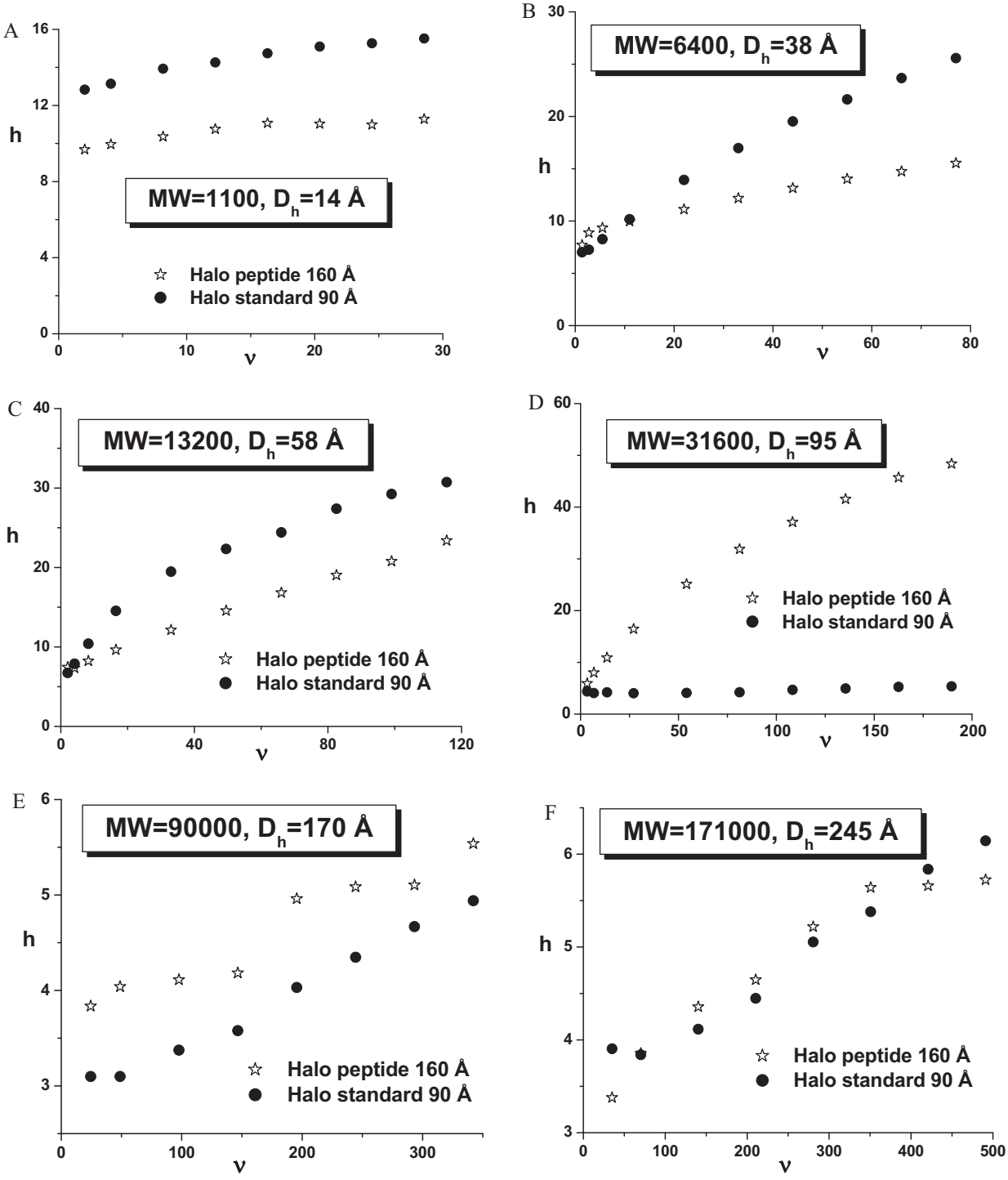

Fig. 9. Plots of the reduced HETP data of six polystyrene standard on the Halo 90 Å (full circles) and Halo-ES-peptide 160 Å (empty stars) columns: (A) *MW* = 1100; (B) *MW* = 6400; (C) *MW* = 13, 200; (D) *MW* = 31, 600; (F) *MW* = 90, 000; (E) *MW* = 171, 000.

($\epsilon_{p,shell}$ = 0.07), the Halo 160 Å ($\epsilon_{p,shell}$ = 0.18), and the Kinetex 100 Å ($\epsilon_{p,shell}$ = 0.13).

4.3. Gradient applications

Fig. 11 illustrates the resolution achieved for a peptide mixture with the new Halo-ES-peptide column. The sample was a tryptic digest of β-lactoglobulin. The flow rate was set at 0.3 mL/min and the initial acetonitrile content was 5%. The acetonitrile concentration was increased linearly at 0.39% per minute. A remarkable peak capacity of 410 was achieved over a 90 min. retention window (average peak width of 13 s). For the sake of comparison, the peak capacity of the Halo 90 Å measured at a flow rate of 0.2 mL/min with a gradient ramp of 0.63% per minute was 370 [10] across the same retention window. Undoubtedly, in agreement with the results found with β-lipotropin, the peak capacity obtained with the new Halo-ES-peptide column are larger than those previously measured with the standard Halo 90 Å column.

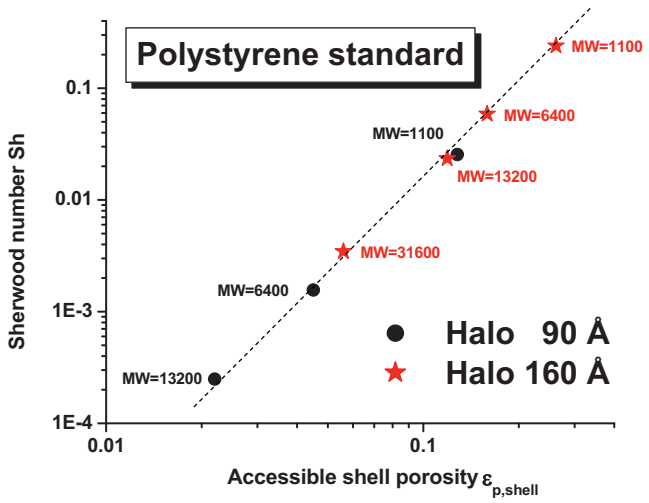

Fig. 10. Plots in a logarithm scale of the experimental Sherwood number as a function of the volume fraction of shell accessible to the polymer with the Halo 90 Å (full squares) and Halo-ES-peptide 160 Å (full stars) columns. Note the strong dependence of the external film mass transfer on the external porosity of the particle.

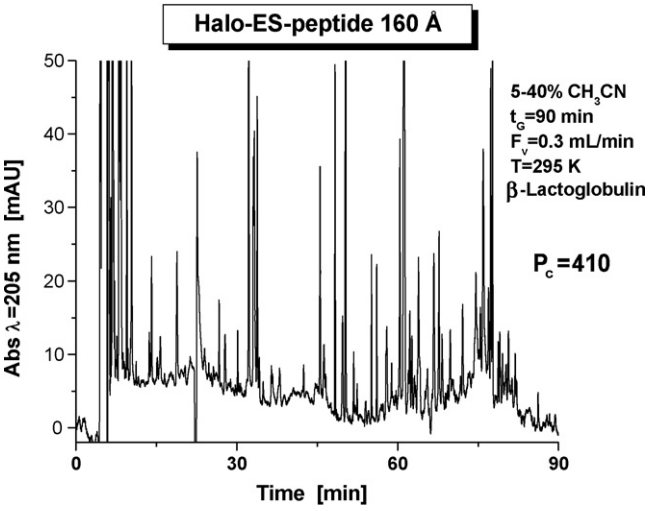

Fig. 11. Resolution of a peptides' mixture (tryptic digest of the protein β-lactoglobulin) on the Halo-ES-peptide 160 Å column. Flow rate: 0.3 mL/min. Gradient: 5% ACN to 40% ACN in 90 min. T = 295 K. The average peak width was about 13 s.

5. Conclusion

Our results demonstrate that the new Halo-ES-peptide (160 Å average pore size) column, designed to resolve mixtures of large molecules, provide markedly better kinetic performance than did the first generation of Halo particles (Halo 90 Å). While this benefit is hardly visible with small molecules, the improvement is most significant with peptide and protein molecules. The kinetic performance for insulin of the 2.7 μm Halo 160 Å particles appears to be equivalent to that of the recently commercialized 2.6 μm Kinetex 100 Å particles.

The physico-chemical explanations for these observations might not necessarily be those anticipated during the design of this new packing material. The initial incentive was to increase the mesopore size in order to reduce the hindrance to diffusion through the porous shells of the particles. Successfully enough, the sample diffusivity in the porous shells was indeed increased (× 1.5 for a non-retained small molecule, uracil, × 3 for the weakly retained peptide, β-lipotropin, and × 6 for a protein, insulin, according to the results of the peak parking measurements). For that all, however, our results prove that the trans-particle mass transfer resistance term is not the limiting kinetic factor that controls the solid–liquid mass transfer resistance in Halo particles. Actually, the van Deemter C term of large molecules is mostly accounted for by a slow external film mass transfer.

By increasing the mesopore size, the manufacturer also increased the fraction of the surface area of the particles that is open to the interstitial eluent and is accessible to the sample molecules (+60% for small molecules, +90% for the peptide, +200% for insulin). The analysis of the kinetic behavior of a series of non-retained polystyrene polymers of different sizes confirms that the external film mass transfer resistance strongly depends on the extent to which these bulky molecules are excluded from the mesoporous volume. We conclude that the improvement of the column efficiency of large molecules such as peptides and proteins (500 < MW < 20, 000 Da) observed with the Halo-ES-peptide column is to be related to the easier access of their molecules to the internal volume. The probability for a molecule to penetrate the shell of the particles increases when its internal porosity increases.

As for small molecules, the improvement in column performance is also due to the eddy diffusion term of the Halo-ES-peptide 160 Å column being 25% smaller than that of the first generation of Halo 90 Å column. This diminution of the A term emphasizes the important role of sample diffusivity through porous particles in the relaxation of radial concentration gradients caused by short-range inter-channel and trans-column velocity biases.

List of symbols

Roman letters

a	EMT parameter defined in Eq. (11)
$A(\nu)$	eddy diffusion term in the reduced van Deemter Eq. (6)
B	longitudinal diffusion coefficient in the reduced van Deemter Eq. (6)
$C(t)$	concentration profile (kg/m^3)
C	overall experimental solid–liquid mass transfer coefficient
C_p	trans-particle mass transfer coefficient in the reduced van Deemter Eq. (6)
C_f	external film mass transfer coefficient in the reduced van Deemter Eq. (6)
D_h	hydrodynamic diameter of the sample molecule (m)
D_{axial}	apparent axial diffusion coefficient in the column (m^2/s)
d_p	average particle size (m)
D_{eff}	effective diffusion coefficient in the porous shell (m^2/s)
D_m	bulk molecular diffusion coefficient (m^2/s)
D_p	particle diffusivity (m^2/s)
D_{pores}	particle diffusivity (m^2/s)
F_ν	inlet flow rate (m^3/s)
$F(\lambda_m)$	hindrance diffusion factor
h	total reduced column HETP
h_{Heat}	additional reduced HETP generated by frictional heating in the column
k_1	zone retention factor
k_0	specific permeability (m^2)
k'	retention factor
k_f	external film mass transfer coefficient (m/s)
K	distribution coefficient between the eluent volume and the solid porous medium
K_c	Kozeny-Carman constant
L	column length (m)
M_i	molecular weight of the eluent i (g/mol)
ΔP	column pressure drop (Pa)
R_c	column inner radius (m)

Sh	Sherwood number
t	time (s)
T	temperature (K)
t_p	parking time (s)
u	interstitial linear velocity (m/s)
u_{PP}	migration linear velocity in the peak parking method (m/s)
V_A	molar volume of the solute at its boiling point (m^3/mol)
x_i	molar fraction of eluent i in the mobile phase

Greek letters

η	eluent's viscosity (Pa s)
ϵ_e	external column porosity
ϵ_p	porosity of the particle after C_{18} derivatization and end-capping
$\epsilon_{p,shell}$	porosity of the shell accessible to the sample molecule
ϵ_t	total column porosity
γ_e	external obstruction factor
$\gamma_{p,shell}$	internal obstruction factor
λ_m	ratio of the sample molecule diameter to the average pore size
μ_1	first moment (s)
μ'_2	second central moment (s^2)
$\mu_{1,ex}$	first moment of the extra-column band profiles (s)
$\mu'_{2,ex}$	second central moment of the extra-column band profiles (s^2)
ν	reduced interstitial linear velocity of the eluent to the particle diameter d_p and bulk molecular diffusion coefficient D_m
Ω	ratio of the intra-particle diffusivity of the sample through the porous shell to the bulk diffusion coefficient
Ψ_i	association factor of the eluent i in the mobile phase
ρ	ratio of the diameter of the solid core to that of the core-shell particle
σ^2_{PP}	variance of the eluted peak in the peak parking experiment (s^2)

Acknowledgements

This work was supported in part by grant CHE-06-08659 of the National Science Foundation and by the cooperative agreement between the University of Tennessee and the Oak Ridge National Laboratory. We thank Jack Kirkland and Joseph di Stefano (Advanced Material Technologies, Wilmington, DE, USA) for the generous gifts of the Halo-C_{18} 160 Å column used in this work and for fruitful discussions.

References

[1] C. Horváth, S.R. Lipsky, Anal. Chem. 7 (1967) 109.
[2] C. Horváth, S.R. Lipsky, J. Chromatogr. Sci. 7 (1969) 109.
[3] J. Kirkland, J. Anal. Chem. 41 (1969) 218.
[4] J. Kirkland, J. Anal. Chem. 64 (1992) 1239.
[5] J.J. DeStefano, T.J. Langlois, J.J. Kirkland, J. Chromatogr. Sci. 46 (2008) 254.
[6] F. Gritti, G. Guiochon, J. Chromatogr. A 1157 (2007) 289.
[7] U. Neue, N. Brady, S. Serpa, P. Iraneta, B. Alden, T. Walter, K. Wyndham, 32nd International Symposium on High Performance Liquid Phase Separations and Related Techniques, Baltimore, MD, May 10–16, 2008.
[8] F. Gritti, G. Guiochon, J. Chromatogr. A 1216 (2009) 1353.
[9] F. Gritti, I. Leonardis, D. Shock, P. Stevenson, A. Shalliker, G. Guiochon, J. Chromatogr. A 1217 (2010) 1589.
[10] F. Gritti, G. Guiochon, J. Chromatogr. A 1217 (2010) 1604.
[11] E. Ol h, S. Fekete, J. Fekete, K. Ganzler, J. Chromatogr. A 1217 (2010) 3642.
[12] J.W. Thompson, R.A. Liberman, J. JW, J. Chromatogr. A 1216 (2009) 7732.
[13] F. Gritti, C. Sanchez, T. Farkas, G. Guiochon, J. Chromatogr. A 1217 (2010) 3000.
[14] F. Gritti, G. Guiochon, J. Chromatogr. A 1217 (2010) 7677.
[15] F. Gritti, I. Leonardis, J. Abia, G. Guiochon, J. Chromatogr. A 1217 (2010) 3219.
[16] F. Gritti, G. Guiochon, J. Chromatogr. A 1217 (2010) 5137.
[17] K. Miyabe, Y. Kawaguchi, G. Guiochon, J. Chromatogr. A 1217 (2010) 3053.
[18] E. Wilson, C. Geankoplis, J. Ind. Eng. Chem. (Fundam.) 5 (1966) 9.
[19] F. Gritti, G. Guiochon, Chem. Eng. Sci. 65 (2010) 6310.
[20] F. Gritti, G. Guiochon, J. Chromatogr. A 1217 (2010) 5069.
[21] B.G. Yew, J. Ureta, R.A. Shalliker, E.C. Drumm, G. Guiochon, AIChE J. 49 (2003) 642.
[22] W. Mandema, H. Zeldenrust, Polymer 18 (1977) 835.
[23] W. Bocian, J. Sitkowski, E. Bednarek, A. Tarnowska, R. Kawecki, L. Kozerski, J. Biomol. NMR 40 (2008) 55.
[24] S.A. Schuster, B.M. Wagner, B.E. Boyes, J.J.J. Kirkland, Chromatogr. Sci 48 (2010) 566.
[25] C. Wilke, P. Chang, AIChE J. 1 (1955) 264.
[26] B. Poling, J. Prausnitz, J. O'Connel, The Properties of Gases and Liquids, 5th ed., McGraw-Hill, New York, NY, 2001.
[27] M. Young, P. Carroad, R. Bell, Biotechnol. Bioeng. 22 (1980) 947.
[28] F. Gritti, M. Martin, G. Guiochon, Anal. Chem. 81 (2009) 3365.
[29] F. Gritti, G. Guiochon, Anal. Chem. 81 (2009) 2723.
[30] K. Kaczmarski, F. Gritti, J. Kostka, G. Guiochon, J. Chromatogr. A 1216 (2009) 6575.
[31] K. Kaczmarski, G. Guiochon, Anal. Chem. 79 (2007) 4648.
[32] R. Landauer, J. Appl. Phys. 23 (1952) 779.
[33] H. Davis, J. Am. Ceram. Soc. 60 (1977) 499.
[34] F. Gritti, G. Guiochon, AIChE J. 57 (2011) 346–358.
[35] J. Giddings, Dynamics of Chromatography, Marcel Dekker, New York, NY, 1965.
[36] F. Gritti, G. Guiochon, Anal. Chem. 78 (2006) 5329.
[37] G. Guiochon, A. Felinger, A. Katti, D. Shirazi, Fundamentals of preparative and nonlinear chromatography, 2nd ed., Academic Press, Boston, MA, 2006.
[38] K. Miyabe, M. Ando, N. Ando, G. Guiochon, J. Chromatogr. A 1210 (2008) 60.
[39] F. Gritti, G. Guiochon, Chem. Eng. Sci. 61 (2006) 7636.
[40] E. Renkin, J. Gen. Physiol. 38 (1954) 225.
[41] F. Gritti, G. Guiochon, J. Chromatogr. A 1128 (2006) 45.
[42] K. Miyabe, G. Guiochon, J. Chromatogr. A 1217 (2010) 3053.
[43] F. Gritti, G. Guiochon, AIChE J. 57 (2011) 333–345.
[44] F. Gritti, G. Guiochon, AIChE J. 56 (2010) 1495.